Mechanical behaviour of biodegradable AZ31 magnesium alloy after long term *in vitro* degradation

Isaiah Adekanmbi [a,1], Christopher Z. Mosher [b], Helen H. Lu [b], Mathis Riehle [c], Haytham Kubba [d], K. Elizabeth Tanner [a,*]

[a] Biomedical Engineering Division, School of Engineering, University of Glasgow, Glasgow G12 8QQ, UK
[b] Department of Biomedical Engineering, Columbia University, New York 10027, USA
[c] Centre for Cell Engineering, University of Glasgow, Glasgow G12 8QQ, UK
[d] Royal Hospital for Sick Children, 1345 Govan Road, Glasgow, G51 4TF, UK

A B S T R A C T

Biodegradable magnesium alloys including AZ31 are exciting candidates for temporary implants as they eliminate the requirement for surgical removal, yet have higher mechanical properties than degradable polymers. However, the very long term mechanical properties and degradation of these alloys have not been fully characterized. The tensile, bending and corrosion behaviour of biodegradable AZ31 Mg alloy specimens have been investigated for up to 9 months *in vitro* in phosphate buffered saline (PBS).
Small AZ31 Mg specimens showed a significant drop in bend yield strength and modulus after 3 months *in vitro* degradation and an average mass loss of 6.1%. Larger dumbbell specimens showed significant drops in tensile strength from 251.96 ± 3.53 MPa to 73.5 ± 20.2 MPa and to 6.43 ± 0.9 MPa and in modulus from 47.8 ± 5.6GPa to 25.01 ± 3.4GPa and 2.36 ± 0.89GPa after 3 and 9 months respectively. These reductions were accompanied by an average mass loss of 18.3% in 9 months.
Degradation rate for the small and large specimens followed similar profiles with immersion time, with peak degradation rates of 0.1747 g m^{-2} h^{-1} and 0.0881 g m^{-2} h^{-1}, and average rates of 0.1038 g m^{-2} h^{-1} and 0.0397 g m^{-2} h^{-1} respectively. SEM fractography and polished specimen cross-sections revealed corrosion pits, cracks and corrosion induced defects. These data indicate the potential of AZ31 Mg for use in implants that require medium term degradation with load bearing mechanical properties.

© 2017 Elsevier B.V. All rights reserved.

1. Introduction

Biodegradable metals are growing in interest as medium term temporary load bearing implants as they provide up to 4 times higher mechanical properties than degradable polymers [1] and longer degradation times. Biodegradable magnesium implants eliminate the need for surgical removal associated with conventional load-bearing implant materials, such as stainless steel, titanium and cobalt-based alloys, and thus reduce the cost of treatment as well as patient morbidity. Magnesium (Mg) and its alloys are particularly useful in orthopaedic surgery due to their Young's moduli (45 GPa) being close to that of bone (7–25 GPa), thus reducing stress shielding, that accelerates bone resorption due to the removal of mechanical stimuli [2,3].

The recent advances with biodegradable Mg alloys have been their use in cardiovascular stents which have undergone human clinical trials [4] and subsequent trials with drug eluting coatings [5]. These stents, made from AE21 magnesium alloy (2% Al, 1% rare earths - Ce, Pr and Nd) were previously used by Heublein et al. [6] to test the degradation kinetics in an *in vivo* study, by implanting the stents into a range of arteries in eleven domestic pigs for 6 months. During the study, intravascular ultrasound images showing a 25% re-enlargement (swelling) of the lumen attributed to loss of mechanical integrity in the AE21 alloy after 35 and 56 days of implantation.

Fracture fixation plates and screws manufactured from commercially pure Mg have also been compared to titanium when used to fix a rabbit ulna fracture model. The fractures healed with full restoration of strength and with new bone formation when Mg implants were used, but not with the control titanium implant [7].

Developments aimed at advancing the performance of biodegradable magnesium based implants by improving their mechanical properties, corrosion resistance and biocompatibility has led to an increase in the range of commercially available Mg alloys. Amongst these alloys, the AZ series of alloys (that is with aluminium and zinc as the alloying elements) have been the most widely used [8] and are now of particular interest as biomaterials. The addition of aluminium (Al) to magnesium

---

* Corresponding author at: Biomedical Engineering Division, School of Engineering, James Watt South Building, University of Glasgow, Glasgow G12 8QQ, UK.
   E-mail address: elizabeth.tanner@glasgow.ac.uk (K.E. Tanner).
[1] Now at DePuy, St Anthony's Road, Leeds LS11 8DT, UK.

Table 1
Chemical composition (wt%) of AZ31 magnesium alloy (data from Magnesium Elektron).

Al	Ca	Cu	Fe	Mn	Ni	Si	Zn	Zr	others
3	<0.005	<0.0005	0.002	0.19	0.0006	0.02	0.71	0.005	<0.3

increases the tensile strength due to grain refinement effects [9] and increases corrosion resistance by forming an Al_2O_3 film on the alloy surface [10]. Zinc (Zn) provides solid solution strengthening and precipitation hardening, but at concentrations of 1–3 wt% can increase the degradation rate. A major limitation with biodegradable Mg and its alloys relates to the potentially rapid degradation rates in physiologically corrosive environments [11] and this may compromise long term mechanical integrity prior to repair of the natural tissue.

To combat this, research on biodegradable magnesium and its alloys has shifted towards coating of these metallic biomaterials using oxide (MgO), fluoride (MgF_2), phosphate (SrP), and apatite based layers (hydroxyapatite) [12–14]. However, such coating interventions provide only a short term 'fix' for implants required for mid-long term applications since the relatively thin coating layer itself eventually degrades leaving the underlying Mg exposed [13].

Despite the recognised need for load bearing implants to provide structural support for a minimum of 3 months [1] and up to 12 months [15], in vitro mechanical degradation of Mg alloys is seldom studied in vitro for longer than 1 month [16–19]. Fu et al. [16] investigated the loss of mechanical properties with AZ31 Mg samples immersed in phosphate buffered saline (PBS) at 37 °C and demonstrated the that corrosion rate of the alloy decreased exponentially with time until it reached a steady rate of 0.05 g m^{-2} h^{-1}. Young's modulus and tensile strength were found to reduce by 10% and 5% respectively over the relatively short timescale of 28 days.

Furthermore, while it is accepted that the corrosion rate of degradable Mg alloys may eventually reach a steady state after several days or weeks of in vitro degradation, a critical feature of the implant material functionality, namely its mechanical properties after extensive degradation periods have not been determined. Thus these previous studies do not provide a complete indication how the mechanical properties of AZ31 degrade in the long term. Bowen et al. [20] degraded commercially pure magnesium wires in vitro in cell culture media for up to 16 days and reported a linear reduction in tensile strength for the bulk samples from 240 MPa at day 0 to 150 MPa at day 13, with spontaneous sample failure occurring at day 14. Weizbauer et al. [21] performed four point bending on in vitro degraded Mg plates of ZEK100 (1% zinc, 0.1% rare earths and 0.1% zirconium) and MgCa0.8 (0.8% Ca) alloys. After 96 h of immersion in Hank's Balanced Salt Solution (HBSS) the bend strength of both alloys was about 7% lower than non-corroded controls, although the degradation rate of MgCa0.8 alloy was noticeably higher than that of the ZEK100 alloy.

Prolonged in vitro studies, that is of multiple months duration, are essential to provide an indication of the long term mechanical behaviour of Mg implants in the physiological environment. However, up until now, there have been no studies on the mechanical properties of AZ31 magnesium after long degradation times. This study characterizes the mechanical properties of AZ31 magnesium alloys after long term (0, 1, 3, 6 and 9 months) in vitro degradation to evaluate its potential for prolonged use in hard and soft tissue implant applications.

2. Materials and methods

2.1. Materials

AZ31 magnesium alloy specimens with a composition of 3% aluminium, 0.71% zinc and 0.19% manganese (Table 1) were obtained from Magnesium Elektron Manchester, UK and used for degradation, tensile and four point bend testing. The zinc content is below the 1–3% range which Staiger et al. [11] suggest leads to increased degradation rates. Test specimens were machined into either rectangular samples 50 × 8 × 2 mm (for 4 point bending tests) with surface area to volume (SA:V) ratio of approximately 2, or dumbbell samples (plate thickness of 2 mm, gauge section 60 mm long by 25 mm) for tensile testing using ISO BSI 6892 [22] with SA:V ratio of approximately 1.

2.2. Degradation test

Specimens were immersed in Phosphate Buffered Saline (PBS) at 37 °C for 3 months for rectangular specimens and 1, 3, 6 or 9 months for dumbbell specimens ($n = 5$ for each time point). The PBS media was generally renewed every 2–3 days, defined as 1 immersion cycle, although occasionally this time had to be extended to 4 or 5 days. These frequent changes in PBS were considered to model better the physiological environment with its stable chemical composition and pH levels. PBS was prepared by mixing 0.2 g KCl, 0.2 g H_2PO_4, 8 g NaCl, 1.15 g Na_2HPO_4 (Sigma Aldrich) in 1000 ml of deionised water [23]. After each immersion cycle the specimens were removed from the PBS, cleaned with distilled water and air dried before weighing using a balance. This enabled calculation of the average mass change and degradation rate. The pH of the degradation media was adjusted to 7.4 ± 0.1 at the start of each immersion cycle and recorded at the end. The volume of the test solution was maintained at 320 ml for rectangular specimens and 4000 ml for dumbbell specimens with one sample in each container. This gave a volume to surface area ratio of 0.40 ml mm^{-2}, according to ASTM G31–72 [24] for the immersion corrosion testing of metals.

The degradation of AZ31 specimens in PBS is governed by the corrosion process ascribed to Mg in aqueous solution.
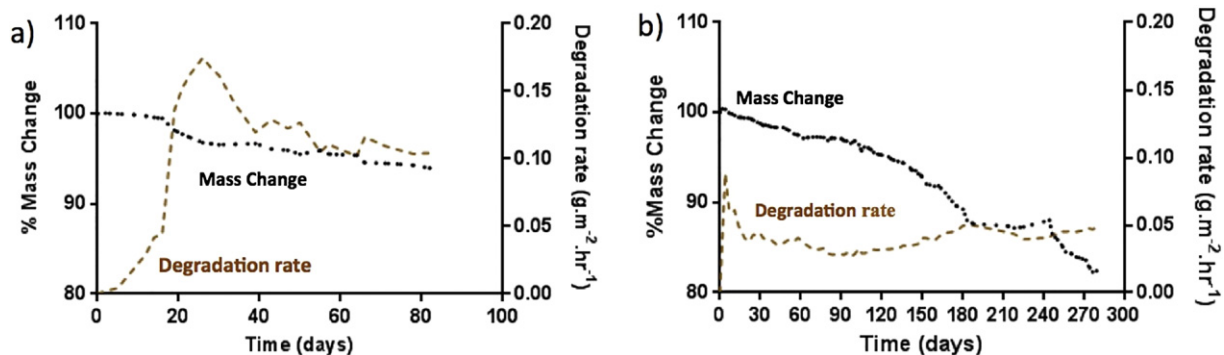
$$Mg + 2H_2O \rightarrow Mg(OH)_2 + H_2 \tag{1}$$

Fig. 1. Degradation rate (dashed brown line) and percentage mass change (dotted black line) of a) AZ31 magnesium rectangular specimens and b) AZ31 magnesium dumbbell samples as a function of immersion time.

Table 2
Maximum, minimum (after maximum degradation rate), final and average degradation rate parameters for AZ31 magnesium rectangular and dumbbell specimens during 3 or 9 months immersion in PBS.

Small rectangular AZ31 Specimens				
	Maximum	Minimum	Final	Average
Time/month	1	2	3	0–3
Mean degradation rate/g m^{-2} h^{-1}	0.1747	0.1019	0.1042	0.1038
Mean penetration rate/mm yr^{-1}	0.87	0.51	0.52	0.52

Large dumbbell AZ31 specimens				
	Maximum	Minimum	Final	Average
Time/month	1	3	9	0–9
Degradation rate/g m^{-2} h^{-1}	0.0881	0.0263	0.0481	0.0397
Penetration rate/mm yr^{-1}	0.44	0.13	0.23	0.19

In the presence of a sodium chloride rich solution this produces

$$Mg(OH)_2 + 2Cl^- \rightarrow MgCl_2 + 2OH^- \tag{2}$$

Mass change (loss) was used to calculate the degradation rate. The mass of each specimen after each immersion cycle (M_i) was divided by its initial mass (M_0) to obtain the normalized mass change (M_i/M_0). The degradation rate (DR) was calculated using Eq. (3).

$$DR = \Delta W/At \tag{3}$$

where ΔW represents the change in sample mass during degradation, A is the original surface area of the sample and t the exposure time. Five specimens were examined per time point and the mean value used to calculate mass loss and degradation rate up to 9 months for the dumbbell specimens and 3 months for the rectangular specimens.

The pH value of the degradation solution was recorded at the end of each immersion cycle throughout the test period. Values of pH were recorded after each immersion cycle using a pH meter (Accument Basic, model AB15) and the average pH of 5 specimens was used.

2.3. Mechanical testing

Flexural properties of rectangular specimens were determined using four-point bend tests. Testing was performed with a uniaxial test machine (MTS810, running TestStar II) fitted with 2.5kN capacity load cell and according to ISO 9585 [25], The separation between the lower or support rollers was 30 mm, while that between the upper or loading rollers was fixed at 10 mm, all rollers were 8 mm diameter. Each specimen was loaded under displacement control at 0.0166 m s^{-1}, using a

pre-load of 2.5 N. Bend yield strength and modulus were calculated using Eqs. (4) to (6).

$$\sigma_f = \frac{F \cdot L}{b \cdot h^2} \tag{4}$$

$$\varepsilon_f = \frac{12 \cdot d \cdot S \cdot h}{L^3} \tag{5}$$

$$E_f = \frac{\Delta \sigma_f}{\Delta \varepsilon_f} \tag{6}$$

where σ_f = bend stress, ε_f = bend strain, E_f = bend modulus, S = specimen deflection or deflection of specimen neutral axis, F = applied load, h = specimen thickness; b = specimen width, L = specimen gauge length, d = the distance between the lower outer roller and upper inner support $\Delta\sigma_f$ = change in bend stress, $\Delta\varepsilon_f$ = change in bend strain,.

Uniaxial tensile tests were performed on non-degraded and degraded AZ31 magnesium dumbbell specimens after 0, 1, 3, 6, or 9 months (initially $n = 5$ for each time point, longer study times had specimen failure during degradation) using an Instron 5984 universal testing machine fitted with 150 kN capacity load cell using an extensometer to measure strain. Tests were performed at room temperature and in accordance with ISO BSI 6892 (BSi EN ISO 6892-1). Each specimen was tested until failure at a displacement rate of 0.033 mm s^{-1}. Force-displacement data was used to calculate stress-strain graphs and to compare mean ultimate tensile strength, tensile strain and tensile modulus at each time point.

2.4. Scanning electron microscopy

Microscopy and fractography was performed using Scanning Electron Microscope (SEM, Zeiss Variable Pressure Analytical SEM with Oxford Microanalysis equipped EDX detector system), allowing observation of the microstructure and composition of fracture surfaces and of polished sections. Also the surface morphology of degraded and non-degraded AZ31 dumbbell specimens was examined, using Digital Elevation Model (DEM) to measure changes in the surface heights. Imaging was performed using a Si detector operating at 20 kV under high vacuum (9.15×10^{-6} Torr, 1.213 kPa), with an objective aperture of 60 µm at two different magnifications. Back Scattered Electron images were taken from the fracture surface of the failed specimen and from a random polished cross sectional area (CSA) remote from the fracture surface. Samples for polishing were embedded in PMMA resin, polished with diamond paste to 1 µm and coated with a 20 nm carbon layer prior to imaging.

2.5. Statistical tests

Statistical analysis (Student's t-test and one-way ANOVA) was performed using Prism version 6 (GraphPad Software, La Jolla, CA).
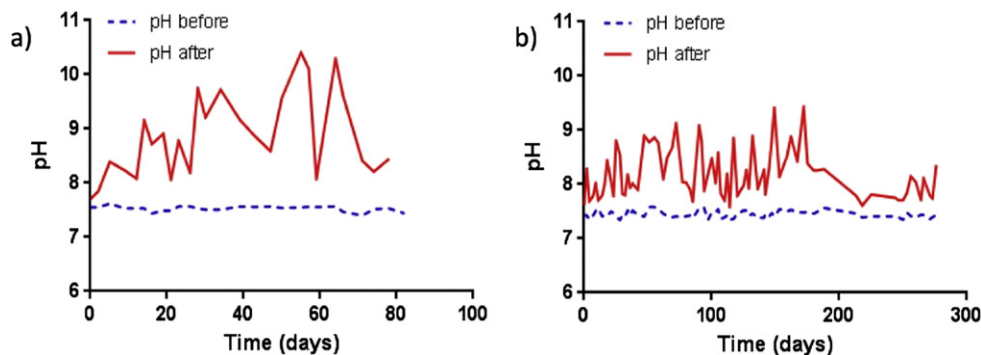

Fig. 2. Degradation media pH for AZ31 Magnesium alloy a) rectangular specimens and b) dumbbell specimens as a function of immersion time before (dashed blue line) and after (solid red line) 2–5 day immersion periods.
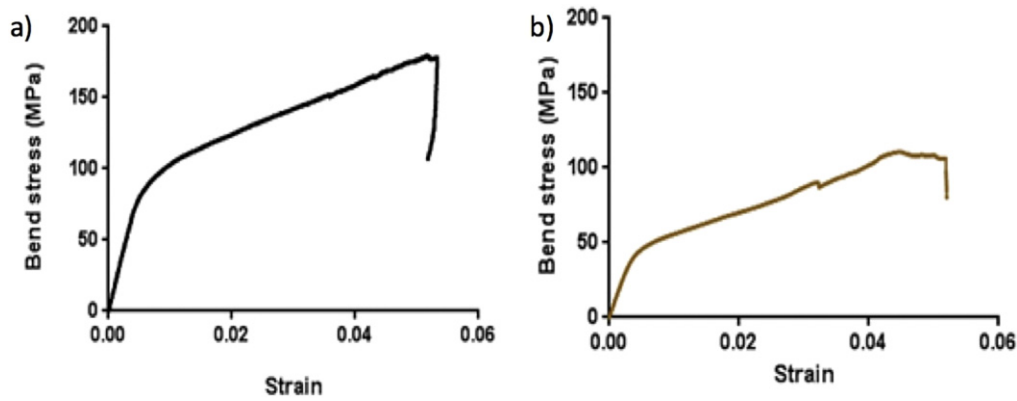
Fig. 3. Typical bending stress-strain curves from rectangular cross section AZ31 magnesium alloy specimens a) before and b) after 3 months *in vitro* degradation in PBS.

3. Results

3.1. Degradation

Fig. 1a presents the mass loss and degradation rate for the small rectangular samples. There was an initial mass gain during the first 2 days immersion. This was followed by a steady mass loss with immersion time so that by day 82 approximately 6.1% of the initial mass was lost. The degradation rate increased rapidly between 0 and 26 days to 0.1746 g m^{-2} h^{-1}. This was followed by a rapid decrease to 0.1019 g m^{-2} h^{-1} at day 39, before fluctuating between 0.1019 and 0.116 g m^{-2} h^{-1} during days 39–66 and finally reaching a slow steady (almost constant) degradation rate of 0.1042 g m^{-2} h^{-1} at day 71 for the remainder of the test period (Table 2).

The mass change and degradation rate of AZ31 dumbbell samples are shown in Fig. 1b. There was an initial mass gain over for the first 2 days of immersion in PBS followed by a gradual mass loss with increasing immersion time so that by day 279 (9 months) approximately 18.3% of the initial mass had been lost. The degradation rate of AZ31 magnesium alloy peaked at 0.0881 g m^{-2} h^{-1} during the first 4 days and then decreased exponentially to a low of 0.0263 g m^{-2} h^{-1} after 96 days before gradually rising to reach a final rate of 0.0481 g m^{-2} h^{-1} after 280 days. Table 2 shows that the degradation rate was highest in month 1 and lowest in month 4 (0.0263 g m^{-2} h^{-1}), giving an average rate over the entire 9 months of 0.0397 g m^{-2} h^{-1}.

Fig. 2a shows the pH measurements for degradation media of the rectangular samples before and after each immersion period. The pH before immersion was regulated at 7.4 ± 0.1 and the pH after individual immersion periods varied between 7.71 ± 0.04 and 10.41 ± 0.77. Fig. 2b shows the equivalent changes for the larger dumbbell specimens. Again it can be observed that degradation media pH increases in alkalinity with increasing immersion cycle. The lowest and highest pH recorded after one immersion cycle (2-5 days) were 7.59 ± 0.05 and 9.43 ± 0.12 after 114 and 172 days respectively.

3.2. Mechanical properties

Stress-strain graphs for degraded and non-degraded specimens were obtained from load deflection curves of the 4 point bend tests (Fig. 3). Both degraded and non-degraded specimens demonstrate a distinct yield behaviour as well as a work hardening zone (linear region) for AZ31 rectangular specimens. After 3 months there was a reduction in ductility during degradation of the specimens. The specimens showed statistically significant drops in yield strength and modulus by 43.98% and 18.54% respectively after 3 months (Fig. 3 and Table 3). No fractures were observed in specimens prior to completion of each bend test since all the specimens made contact with support rollers before fracture and this did not allow the measurement of ultimate bend strength, but did indicate that the material was ductile and underwent significant amounts of plastic deformation.

Force-displacement data obtained from uniaxial tension tests were used to determine tensile stress-strain behaviour and mechanical properties. In tension, similar to the bend testing, work hardening behaviour was observed and it was evident that with increasing degradation time the length of the work hardening deformation zone (necking region of specimen) and thus the ductility of the material decreased (Fig. 4). The average ultimate tensile strength and Young's modulus before and after degradation are shown in Table 4. Non-degraded groups showed the highest modulus (47.8 ± 5.68GPa) and tensile strength (251.96 ± 3.53 MPa). With degradation time, both tensile modulus and strength decreased. The greatest drop in modulus occurred between months 3 and 6, whereas the greatest drop in tensile strength occurred between month 1 and month 3. Tensile strain at failure decreased with increasing immersion time and was highest in non-degraded samples (10.86%) and lowest after 9 months (0.5%) (Table 4). For non-degraded samples a clear and distinctive yield region was observed followed by specimen fracture. In specimens degraded for 6 and 9 months however, there was minimal yield behaviour prior to fracture and this was shown by a very small yield region.

3.3. AZ31 surface morphology

Optical micrographs (Fig. 5) show the effect of corrosion on the surface topography after 0, 1, 3, 6 and 9 months immersion in PBS. The transformation from a smooth to rough surface and the noticeable color change from shiny silver to white and dark grey indicate the formation of non-metallic (oxide) phases on and within the specimens as immersion time increases.

The surface degradation morphology before and after immersion in PBS is shown in Fig. 6. Non-degraded specimens were free from surface cracks and pits. The degradation behaviour is characterized by pitting followed by corrosion induced cracks. Deep corrosion pits had formed by 3 months and reached up to 6 mm in diameter by 9 months as shown by SEM. These defects penetrate the surface layer and by month 9 reached approximately 800 μm into the specimen as measured using DEM on the SEM. Visual observation showed corrosive attack by the solution increased at the specimen corners.
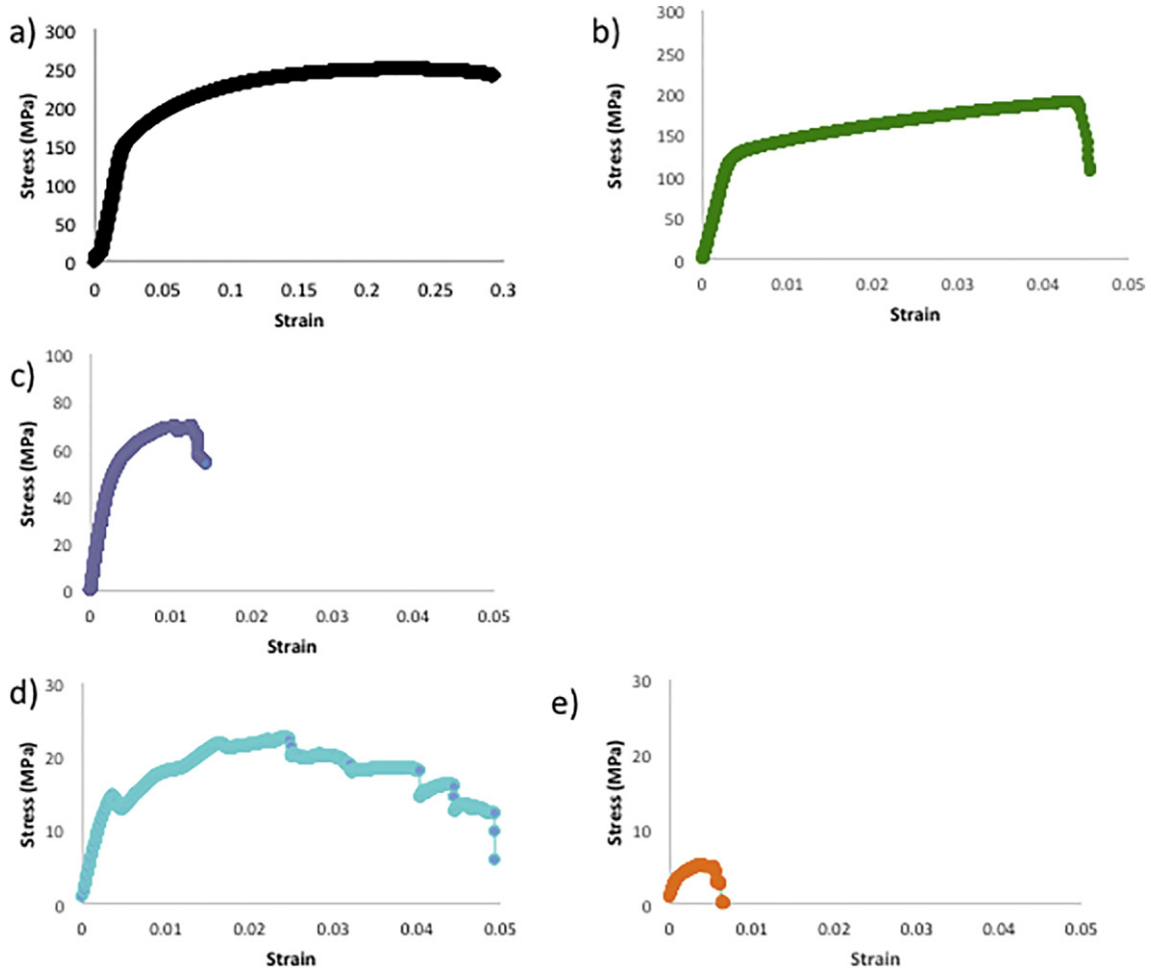
Table 3
Bending properties of AZ31 Magnesium alloy rectangular specimens after 0, and 3, months of *in vitro* degradation in PBS. Values shown are mean ± standard deviation.

Degradation time/months	Bend yield stress/MPa	Bend modulus/GPa	Number of specimens tested
0	84.55 ± 4.28	34.77 ± 1.54	5
3	47.37 ± 5.91	28.33 ± 2.84	4

Fig. 4. Typical tensile stress-strain behaviour for AZ31 magnesium alloy after a) 0, b) 1, c) 3, d) 6 and e) 9 months of *in vitro* degradation in PBS. Data from a median sample in each group.

Formation of an irregular film over the surface of corroded specimens was also observed very early on (within a few days of immersion) and this was most noticeable when rinsing individual specimens.

3.4. Fractography

Backscattered Electron Images (BEI) show surface morphology and cross sectional views in polished and unpolished samples after various degradation times. In BEI, areas which appear lighter indicate non-corroded metallic rich regions, while darker areas indicate metal oxide regions and corrosion products. Manifestations of metal oxide formation (Fig. 7A), corrosion induced cracks (Fig. 7B) and development of corrosion products (Fig. 7C) increased in severity with increasing immersion time in PBS. The corrosion induced cracks appear predominantly in metal oxide regions. Observation of the fracture surfaces revealed that corrosion pits increased in depth with increasing time from 20 to 30

μm after 1 month to a depth of up to 800 μm for the 9 month samples. Examination of cross sections (Fig. 7C) shows that the corrosion product forms a thin layer, covering the sample surface within the first month of immersion and progressively growing deeper into the specimen core with increasing time. By the end of 9 months, the metallic regions of the degraded specimens were almost fully replaced with corrosion product across the entire specimen thickness.

3.5. Elemental analysis of AZ31 cross sections

Fig. 8a is an aggregate image of the dot maps (Fig. 8b–i) superimposed over a randomly selected SEM image after 6 months degradation in Fig. 7C. The SEM shows that degradation has occurred simultaneously from both sides of the sample at this region. In the upper part there is only transformation of the material, without obvious loss of material, but in the lower part there is more extensive degradation and

Table 4
Tensile properties of AZ31 Magnesium alloy dumbbell specimens after 0, 1, 3, 6 or 9 months of *in vitro* degradation in PBS. Values shown are mean ± standard deviation.

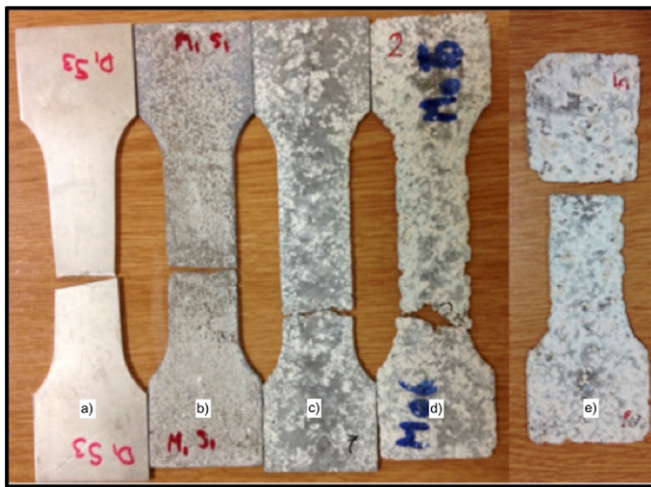| Degradation time/months	Ultimate tensile strength/MPa	Strain at fracture/%	Tangent modulus/GPa	Tensile yield stress/MPa	Number of specimens tested
0	251.96 ± 3.53	10.86 ± 3.47	47.80 ± 5.68	162.11 ± 33.38	5
1	188.69 ± 18.70	4.23 ± 1.84	41.88 ± 1.56	121.84 ± 4.36	4
3	73.52 ± 20.22	2.79 ± 0.38	25.01 ± 3.42	63.22 ± 19.31	4
6	34.23 ± 7.60	1.25 ± 0.26	4.02 ± 2.69	13.42 ± 7.34	4
9	6.43 ± 0.95	0.50 ± 0.20	2.36 ± 0.89	5.93 ± 2.50	3

Fig. 5. Optical micrographs of AZ31 dumbbell specimens after a) 0, b) 1, c) 3, d) 6 and e) 9 months immersion in PBS and tensile testing. The gap in sample d) was lost during the mechanical testing and part of sample e) has been removed for SEM and thus only one fracture occurred.

nearest the surface there is also loss of material. The light green areas of the image indicate regions of non-degraded magnesium alloy. The sample surface corrosion layer depicted by the red, bright purple, yellow and orange regions, (also seen in Fig. 8c, d, f, g) is rich with oxygen, phosphorus, carbon and calcium respectively, indicating the presence of a phosphate (PO_4^{3-}) based external layer precipitated over the entire surface and oxygen indicating MgO throughout the corroded region. Areas appearing light and dark teal, and dark purple (Fig. 8e, h, i) indicate regions rich with aluminium, zinc and manganese respectively, the main alloying elements (Table 1). The corroded region which appears at the centre of each image penetrates the specimen core and consists mainly of the phosphorus, oxygen, carbon, calcium, magnesium, aluminium and potassium, indicating the formation of MgO and Mg replaced phosphate (PO_4^{3-}) phases. Traces of sodium and chlorine can also be observed deep within the sample core and are from the degradation solution.

4. Discussion

AZ31 magnesium alloy is becoming an increasingly attractive biomaterial for temporary medical implants because of its mechanical, degradation and biocompatibility characteristics. However, the long term mechanical properties (at least 6 months degradation) have not been characterized. Here we show, for the first time, the reduction in mechanical properties after many months *in vitro* degradation. Decreasing tensile properties with increasing degradation time was observed. Tensile strength, tensile yield stress and modulus decreased significantly by month 3 (reductions of 70.8%, 61% and 47.6% respectively) and through to month 9 (reductions of 97.4%, 96.3% and 95%) (Fig. 4) in PBS.

Despite the considerable drop in tensile properties after 3, 6 and 9 months of *in vitro* degradation it is evident that the tensile modulus after 6 months of *in vitro* degradation is (4.02 ± 2.69GPa) still noticeably higher than that of commonly used biodegradable polymers at the time of implantation (0.36–1.8GPa). The observed reduction in tensile strain with immersion time (Fig. 4 and Table 4) indicates the gradual transition from a ductile to a more brittle failure mode for the AZ31 dumbbell specimens and this was further confirmed in fully degraded specimens which exhibited minimal necking compared with non-degraded specimens.

To date, there have been no comparable reports on the long term change in mechanical properties of biodegradable magnesium alloys.

However, Fu et al. [16] investigated the uniaxial tensile properties and fatigue behaviour of AZ31 dumbbell specimens in PBS over 28 days. The tensile modulus and elongation of AZ31 specimens reduced with increasing immersion time by 10% and 20% respectively and the fatigue life was reduced by a factor of 2.5–5 [16]. This closely reflects data from our present study where there was a 12.8% drop in tensile modulus during the first month.

For AZ31 Mg alloys, the reduction in tensile yield stress and tensile modulus after 3 months of degradation was greater than those in bend yield stress and bend modulus by 17.1% and 29.2% respectively. These results suggest that AZ31 Mg alloy may be better suited for biomaterial implant applications that require mid to long term mechanical bend resistance as opposed to tensile resistance when exposed to physiological environments.

Four-point bending was chosen rather than three-point since the former produces peak stresses over a larger region of the specimen. This gives more relevant measurements, particularly in the presence of pitting corrosion which is non-uniform over the surface. Weizbauer et al. [21] used the same test configuration for MgCa0.8 and ZEK100 Mg alloys and found a similar relationship, that is, a non-statistically significant drop (7%) in bend strength with degradation time after 96 h immersion in Hank's balanced salt solution. The apparently low bend modulus in comparison to the tensile modulus may be ascribed firstly, to the different test geometries used in both techniques, secondly to the assumption that with bending tests compressive modulus is identical to tensile modulus at the neutral axis and in practice the compressive modulus of magnesium and its alloys is known to be lower than the tensile modulus [26].

An initial small mass gain was observed for both specimen shapes (Fig. 1) and may be attributed to an early build-up of corrosion products forming a protective hydroxide film layer on the magnesium surface. Thereafter, both AZ31 specimen geometries exhibited a continuous, but gradual, mass loss with immersion time due to the on-going processes of a corrosion product surface layer gradually forming on the specimens and then dissolving away.

Degradation rate was measured using an immersion method according to ASTM G31–72 [24]. The degradation rate for magnesium alloys may differ by up to 3 orders of magnitude [19], depending on experimental factors. Where volume effects are important, it can be more suitable to express degradation rates from mass loss (g m^{-2} h^{-1}) experiments in the form of corrosion penetration rates (mm yr^{-1}). For AZ31 alloy, *in vitro* corrosion penetration rates have been shown to vary between 0.3 and 6.99 mm yr^{-1}, with the lower rate appearing in a study that used immersion in Hank's balanced salt solution for 10 days and the higher penetration rate coming from a study which used an electrochemical method with 3.5% NaCl solution for 24 days [27].

In this current study, it can be inferred from the relatively low degradation rates measured for large dumbbell (0.13–0.44 mm yr^{-1}) and small rectangular (0.51–0.87 mm yr^{-1}) AZ31 specimens that only small quantities of Mg metal ions are released into the degradation solution with time, indicating that AZ31 degradation products should be excreted from the physiological environment [17] without compromising tissue metabolism.

A number of factors may influence the *in vitro* degradation rates obtained for Mg alloys. For instance; the size and geometry of samples used, the choice of degradation solution, the temperature and CO_2 environment used and the time between the renewal of the degradation media [19,28]. However, minimum and approximate steady state values for the degradation rate of rectangular specimens (SA:V ratio 2.3) obtained in this study (0.10 g m^{-2} h^{-1}) are comparable to those described by Fu et al. [16] who immersed small dumbbell specimens of AZ31 (SA:V ratio 1.8) in PBS and reported a low steady state corrosion rate of 0.05 g m^{-2} h^{-1} over 30 days. The discrepancies between the mass loss and degradation rate profile between rectangular and dumbbell samples can be attributed to the different surface area to volume ratios
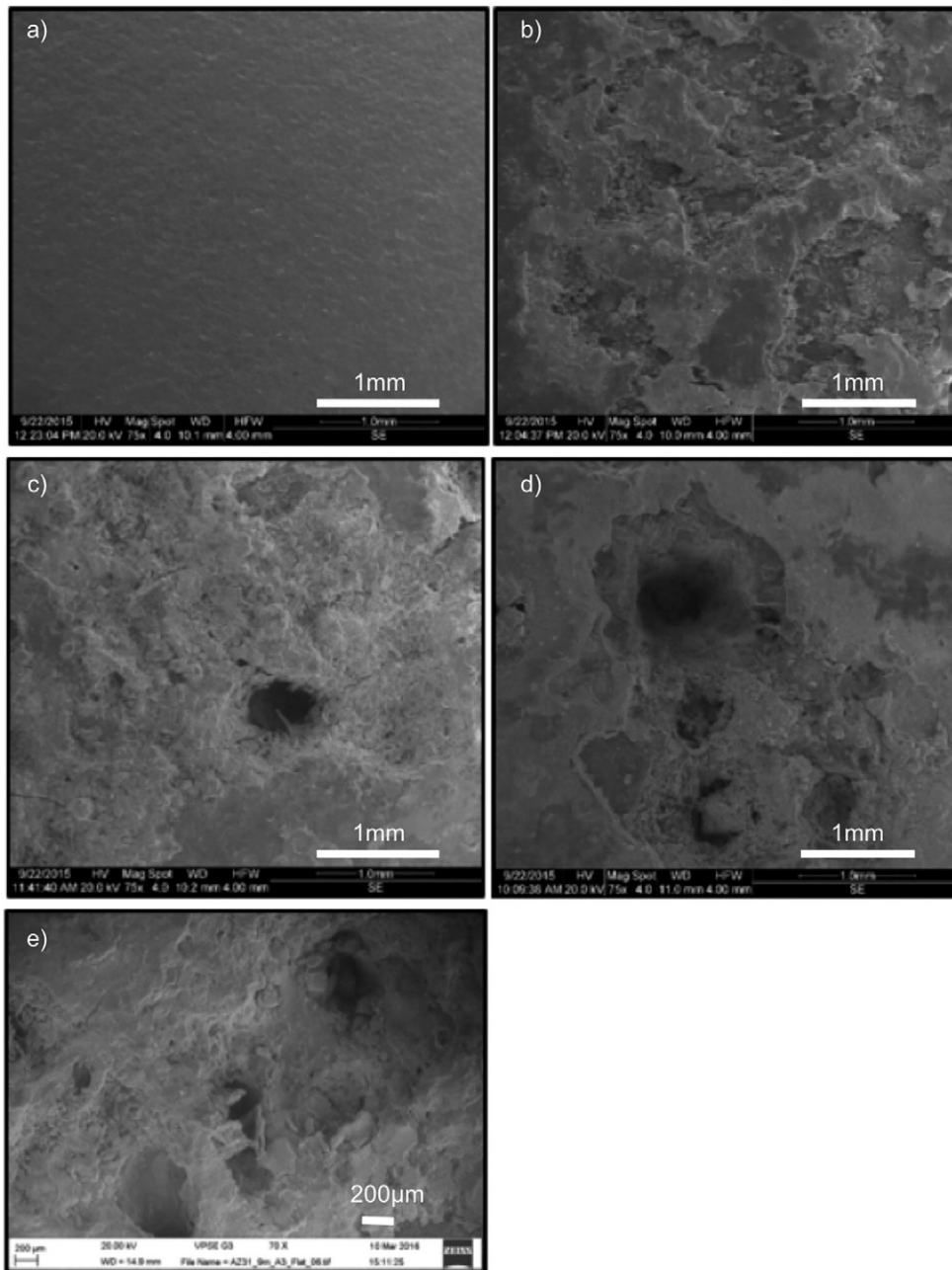
Fig. 6. SEM images showing surface morphology in AZ31 dumbbell samples and the development of corrosion pits on the sample surface in a) non-degraded and degraded specimens after b) 1 month, c) 3 months, d) 6 months and e) 9 months of immersion in PBS (scale bars indicated on image as 1 mm or 200 μm).

used for each, with smaller rectangular samples having higher SA:V ratio of 2.3:1 and larger dumbbell specimens having a ratio of 1.1:1.

The degradation solution pH at the end of each immersion cycle became more alkaline, fluctuating between 7.59 ± 0.05 and 9.43 ± 0.12 for the dumbbell specimens and 7.71 ± 0.04 and 10.41 ± 0.77 for the smaller rectangular specimens. Any changes in the degradation media pH will ultimately produce a more corrosive environment [29] and accelerate the degradation processes. The variations in the pH values at the end of each immersion cycle were considered to be due to variations in how well and firmly the deposited layer covered the surface, thus how much degradation occurred during each immersion cycle. More recently, research on reducing the degradation of Mg alloys have focused on coating interventions as a means of controlling the degradation rate. These surface modifications are typically based on slowing down the anodic dissolution in physiological solution, or by the deposition of biocompatible material layers such as MgF_2, MgO, SrP, hydroxyapatite, or strontium apatite [12,13].

While such coating interventions have been reported to improve the degradation resistance compared to non-coated Mg surfaces [14], the effects are often short lived since the coating layer eventually corrodes away leaving the underlying Mg exposed. The effectiveness of these coating techniques can further be rapidly diminished due to cracking of the coating during deformation. Coating interventions are therefore unlikely to significantly benefit the long term degradation resistance of magnesium and a better understanding of the mechanical behaviour of non-coated magnesium alloys after long term degradation is essential for complete characterization of the expected performance when implanted for medium to long term applications.

Above pH 11.5 a protective hydroxide film will form over the surface of Mg. During our study, this phenomenon was prevented by renewing
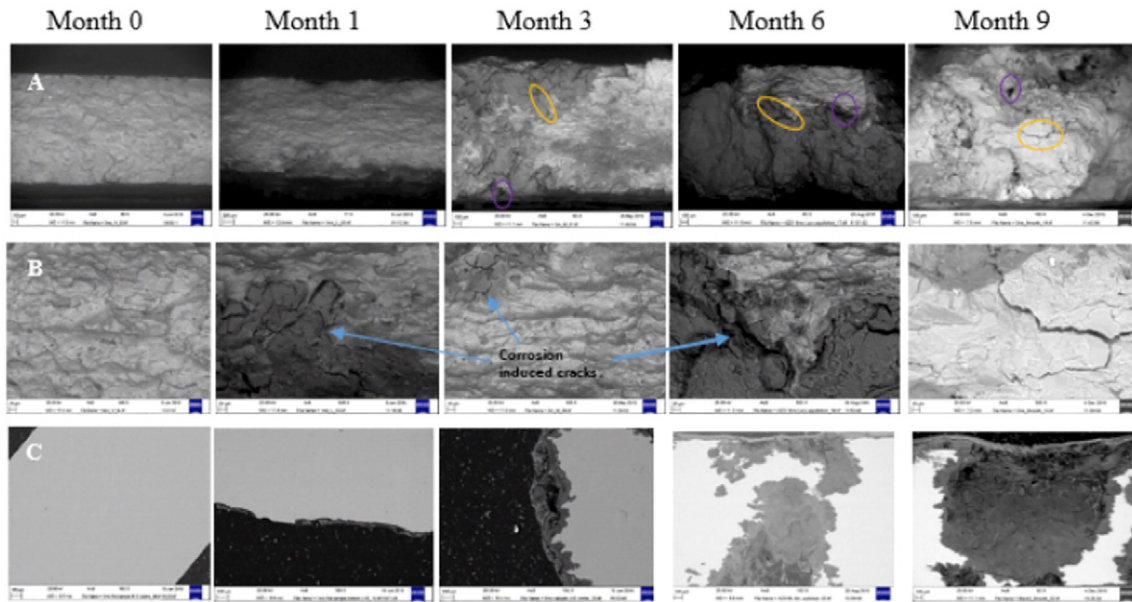
Fig. 7. SEM of AZ31 dumbbell samples showing tensile fracture surface morphology after 0, 1, 3, 6, or 9 (left to right) months immersion in PBS A) low magnification (marker bars = 100 μm) and B) high magnification (marker bars = 20 μm). C) polished sample cross sections remote from the tensile fracture site (marker bars = 100 μm). Regions highlighted with yellow circles and purple ovals indicate regions of magnification and corrosion pits.

the PBS degradation solution every 2-5 days and buffering to 7.4 ± 0.1. In the physiological environment such an accelerated degradation effect is efficiently mitigated since physiological fluids are continuously replenished. Furthermore, a natural buffering mechanism exists which uses bicarbonate ions, carbon dioxide (CO_2) and carbonic acid to counteract hydroxide and H^+ ions which may otherwise cause excessive shifts in physiological pH [30]. This may explain why degradation of Mg based metals is reported to be 4 times faster *in vitro* than *in vivo* [18].

Eqs. (1) and (2) illustrate that degradation of Mg alloys can produce a number of by-products such as dissolved Mg ions, hydroxyl ions (OH^-) and hydrogen gas (H_2) and these products invariably alter the pH of the degradation solution. However, as already mentioned, it is often necessary to add buffering agents (HPO_4^{2-}, HCO_3^- and HCl) when replenishing manually formulated *in vitro* degradation solutions (for example PBS) [19] and this may account for the large variations in measured pH after immersion for both geometries of AZ31 Mg specimens.

Microstructural analysis of the AZ31 dumbbell sample cross-sections after various immersion times revealed evidence of pitting corrosion and evolution of these specimen topographies were shown to increase with degradation time (Fig. 7). Pitting corrosion is a localised corrosive attack which forms small cavities or pits on a horizontal surface that grow downwards into a material, and stress corrosion cracking is the propagation of a crack by combination of an applied stress and a corrosive environment [31]. These corrosion induced flaws, which are common in magnesium alloys [32], act as precursors for mechanical failure and appeared predominantly in the metal oxide regions. Often with metals, corrosion pits can be obscured by a corrosion product layer which covers the metallic surface, and this sometimes makes pitting corrosion undetectable and particularly difficult to predict or to design against. Crack formation in the metal oxide regions is a characteristic feature of failure in brittle materials and commonly associated with catastrophic mechanical fracture. Such behaviour is atypical in ductile AZ31 alloys which undergo noticeable necking and deformation prior to failure [8], but can be introduced by factors in the metals external environment. Elemental analysis with X-ray mapping (Fig. 8) revealed the distribution of elements and the distinct difference between the composition of the pitting corrosion regions, the non-corroded regions and the surface covered by mineralised phosphate.

A limitation of this study was the static degradation environment used as part of the *in vitro* model which may create a more detrimental local pH environment compared with that presented in the dynamic physiological environment of the body. Toxicologically, one concern with aluminium containing Mg alloys is the link with neurotoxic related illnesses such as Alzheimer's diseases due to the ability of Al to pass through the blood-brain barrier. However, when introduced into the body in small quantities for instance, during dietary ingestion [33], or consumption from natural or urban water supplies [34], Al is naturally excreted through urine or in the form of bile [35]. This seems promising given the relatively low degradation rate measured in this study and the low Al content for AZ31 magnesium specimens compared with other Mg-Al alloys.

5. Conclusions

The tensile and bend strength and modulus of AZ31 Mg allow after long term degradation have been quantified.

The AZ31 magnesium specimens retain 56.0% and 81.5% of their bend yield strength and bend modulus and 38.9% and 52.3% of their tensile yield and tensile modulus respectively after 3 months degradation and retain 3.7% and 4.9% of their tensile yield and tensile modulus respectively after 9 months in PBS. Despite this, the modulus of AZ31 after 9 months degradation was still higher than those of commonly used bioresorbable polymers before degradation.

The peak degradation rates were 0.1747 g m^{-2} h^{-1} and 0.0881 g m^{-2} h^{-1} for small and large samples respectively. The mean degradation rates were 0.1038 g m^{-2} h^{-1} and 0.0397 g m^{-2} h^{-1} and these relatively low values indicate that only small quantities of metal ions dissolve into the degradation solution with time.

Our study provides indications for the expected long term performance of AZ31 magnesium alloy for biodegradable implant applications that serve to provide structural and mechanical support for biological tissue over several months.
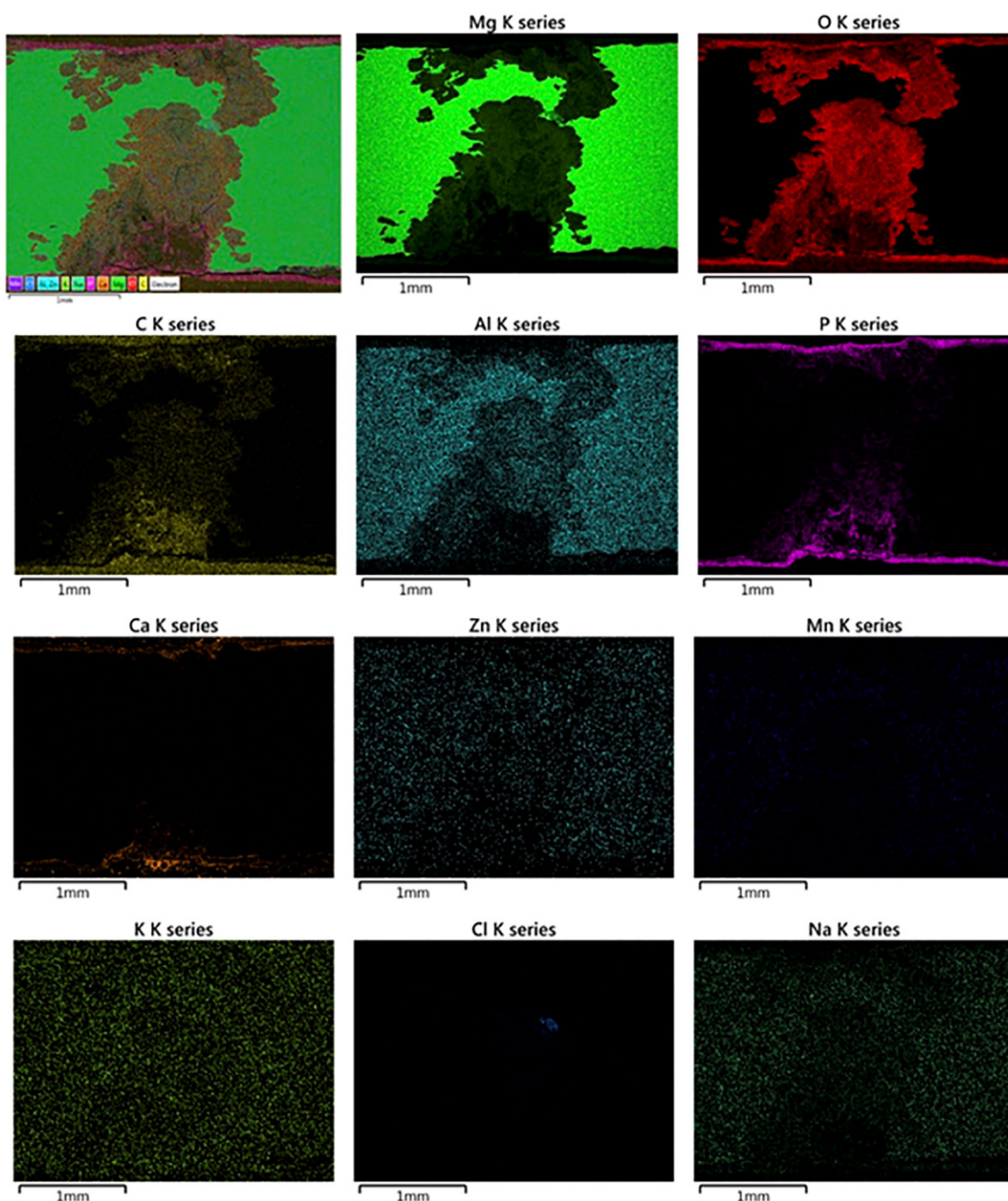
Fig. 8. Elemental analysis and X-ray dot mappings of AZ31 dumbbell sample after 6 months immersion in PBS. Illustrating the composition of elements in the corrosion product at the fracture surface and in surface corrosion film layer (all marker bars = 1 mm).

References

[1] F. Witte, V. Kaese, H. Haferkamp, E. Switzer, A. Meyer-Lindenberg, C.J. Wirth, H. Windhagen, In vivo corrosion of four magnesium alloys and the associated bone response, Biomaterials 26 (2005) 3557–3563, http://dx.doi.org/10.1016/j.biomaterials.2004.09.049.

[2] H. Brar, M.O. Platt, M. Sarntinoranont, P.I. Martin, M.V. Manuel, Magnesium as a biodegradable and bioabsorbable material for medical implants, J. Miner. Met. Mater. Soc. 61 (2009) 31–34, http://dx.doi.org/10.1007/s11837–009–0129-0.

[3] S.J. Mellon, K.E. Tanner, Mechanical adaptability of bone in vivo and in vitro – a review, Int. Mater. Rev. 25 (2012) 235–255, http://dx.doi.org/10.1179/1743280412Y.0000000008.

[4] R. Waksman, R. Erbel, C. Di Mario, J. Bartunek, B. de Bruyne, F.R. Eberli, et al., Early- and long-term intravascular ultrasound and angiographic findings after bioabsorbable magnesium stent implantation in human coronary arteries, JACC Cardiovasc. Interv. 2 (2009) 312–320, http://dx.doi.org/10.1016/j.jcin.2008.09.015.

[5] R. Waksman, F. Prati, N. Bruining, M. Haude, D. Bose, H. Kitabata, P. Erne, S. Verheye, H. Degen, P. Vermeersch, et al., Serial observation of drug-eluting absorbable metal scaffold multi-imaging modality assessment, Circ. Cardiovasc. Interv. 6 (2013) 644–653, http://dx.doi.org/10.1161/CIRCINTERVENTIONS.113.000693.

[6] B. Heublein, R. Rohde, V. Kaese, M. Niemeyer, W. Hartung, A. Haverich, Biocorrosion of magnesium alloys: a new principle in cardiovascular implant technology? Heart 8 (2003) 651–656, http://dx.doi.org/10.1136/heart.89.6.651.

[7] A. Chaya, S. Yoshizawa, K. Verdelis, N. Myers, B.J. Costello, D.-T. Chou, S. Pal, S. Maiti, P.N. Kumta, C. Sfeir, In vivo study of magnesium plate and screw degradation and

bone fracture healing, Acta Biomater. 18 (2015) 262–269, http://dx.doi.org/10.1016/j.actbio.2015.02.010.

[8] M. Marya, L.G. Hector, R. Verma, W. Tong, Microstructural effects of AZ31 magnesium alloy on its tensile deformation and failure behaviors, Mater. Sci. Eng., A 418 (2006) 341–356, http://dx.doi.org/10.1016/j.msea.2005.12.003.

[9] F. Witte, N. Hort, C. Vogt, S. Cohen, K.U. Kainer, R. Willumeit, F. Feyerabend, Degradable biomaterials based on magnesium corrosion, Curr. Opin. Solid State Mater. Sci. 12 (2008) 63–72, http://dx.doi.org/10.1016/j.cossms.2009.04.001.

[10] Y.F. Zheng, X.N. Gu, F. Witte, Biodegradable metals, Mater. Sci. Eng. R. Rep. 77 (2014) 1–34, http://dx.doi.org/10.1016/j.mser.2014.01.001.

[11] M. Staiger, A.M. Pietak, J. Huadmai, G. Dias, Magnesium and its alloys as orthopedic biomaterials: a review, Biomaterials 27 (2006) 1728–1734, http://dx.doi.org/10.1016/j.biomaterials.2005.10.003.

[12] X.B. Chen, D.R. Nisbet, R.W. Li, P.N. Smith, T.B. Abbott, M.A. Easton, D.H. Zhang, N. Birbilis, Controlling initial biodegradation of magnesium by a biocompatible strontium phosphate conversion coating, Acta Biomater. 10 (2014) 1463–1474, http://dx.doi.org/10.1016/j.actbio.2013.11.016.

[13] B.J. O'Brien, W.M. Carroll, A.J. Conneely, G.M. O'Connor, Combined anodizing and picosecond laser treatment to control the corrosion rate of biodegradable magnesium alloy AZ31, Proc. I. Mech. E. Pt. L: J. Mater. Design App, 228, 2014, pp. 278–287, http://dx.doi.org/10.1177/1464420713487648.

[14] T.T. Yan, L.L. Tan, D.S. Xiong, X.J. Liu, B.C. Zhang, K. Yang, Fluoride treatment and in vitro corrosion behavior of an AZ31B magnesium alloy, Mater. Sci. Eng., C 30 (2010) 740–748, http://dx.doi.org/10.1016/j.msec.2010.03.007.

[15] H. Hermawan, D. Dubé, D. Mantovani, Developments in metallic biodegradable stents, Acta Biomater. 6 (2010) 1693–1697, http://dx.doi.org/10.1016/j.actbio.2009.10.006.

[16] S. Fu, H. Gao, G. Chen, L.L. Gao, X. Chen, Deterioration of mechanical properties for pre-corroded AZ31 sheet in simulated physiological environment, Mater. Sci. Eng., A 593 (2014) 153–164, http://dx.doi.org/10.1016/j.msea.2013.11.012.

[17] Y. Ren, J. Huang, B. Zhang, K. Yang, Preliminary study of biodegradation of AZ31B magnesium alloy, Front. Mater. Sci. Chin. 1 (2007) 401–404.

[18] F. Witte, J. Fischer, J. Nellesen, H.A. Crostack, V. Kaese, A. Pisch, F. Beckmann, H. Windhagen, In vitro and in vivo corrosion measurements of magnesium alloys, Biomaterials 27 (2006) 1013–1018, http://dx.doi.org/10.1016/j.biomaterials.2005.07.037.

[19] Y. Xin, T. Hu, P.K. Chu, In vitro studies of biomedical magnesium alloys in a simulated physiological environment: A review, Acta Biomater. 7 (2011) 1452–1459, http://dx.doi.org/10.1016/j.actbio.2010.12.004.

[20] P.K. Bowen, J. Drelich, J. Goldman, A new in vitro-in vivo correlation for bioabsorbable magnesium stents from mechanical behavior, Mater. Sci. Eng. C 33 (2013) 5064–5070, http://dx.doi.org/10.1016/j.msec.2013.08.042.

[21] A. Weizbauer, C. Modrejewski, S. Behrens, H. Klein, P. Helmecke, J.M. Seitz, H. Windhagen, K. Mohwald, J. Reifenrath, H. Waizy, Comparative in vitro study and biomechanical testing of two different magnesium alloys, J. Biomater. Appl. 28 (2014) 1264–1273, http://dx.doi.org/10.1177/0885328213506758.

[22] BSi EN ISO 6892-1 Metallic Materials, Tensile Testing Part 1: Method of Test at Room Temperature, 2014.

[23] M. Alvarez-Lopez, M.D. Pereda, J.A. del Valle, M. Fernandez-Lorenzo, M.C. Garcia-Alonso, O.A. Ruano, M.L. Escudero, Corrosion behaviour of AZ31 magnesium alloy with different grain sizes in simulated biological fluids, Acta Biomater. 6 (2010) 1763–1771, http://dx.doi.org/10.1016/j.actbio.2009.04.041.

[24] ASTM-G31-72 Standard Practice for Laboratory Immersion Corrosion Testing of Metals, Annual Book of ASTM Standards Philadelphia, Pennsylvania, USA, American Society for Testing and Materials, 2004.

[25] D. Cesarone, J.A. Disegi, Techniques in the application of ISO 9585 test method for the determination of bone plate bending properties, in: J.P. Harvey, R.F. Games (Eds.), Clinical and Laboratory Performance of Bone Plates, West Conshohocken, PA, ASTM International 1994, pp. 65–71.

[26] H. Kato, Y. Tottori, K. Sasaki, Four-point bending test of determining stress-strain curves asymmetric between tension and compression, Exp. Mech. 54 (2014) 489–492, http://dx.doi.org/10.1007/s11340-013-9791-9.

[27] A.H.M. Sanchez, B.J.C. Luthringer, F. Feyerabend, R. Willumeit, Mg and mg alloys: how comparable are in vitro and in vivo corrosion rates? A review, Acta Biomater. 13 (2015) 16–31, http://dx.doi.org/10.1016/j.actbio.2014.11.048.

[28] R. Willumeit, F. Feyerabend, N. Huber, Magnesium degradation as determined by artificial neural networks, Acta Biomater. 9 (2013) 8722–8729, http://dx.doi.org/10.1016/j.actbio.2013.02.042.

[29] M. Pourbaix, Atlas of Electrochemical Equilibria in Aqueous Solutions, 2nd English ed. National Association of Corrosion Engineers, Houston, 1974.

[30] N. Kirkland, N. Birbilis, Magnesium biomaterials design, testing, and best practice, Magnesium Biomaterials: Design, Testing, and Best Practice, Book Series: Springerbriefs in Materials, 2013, pp. 1–132.

[31] W. Callister, Materials Science and Engineering: An Introduction (6th Sixth Ed.), John Wiley and Sons Inc., 2003

[32] G.L. Song, A. Atrens, Corrosion mechanisms of magnesium alloys, Adv. Eng. Mater. 1 (1999) 11–33.

[33] A. Proudfoot, Aluminium and zinc phosphide poisoning, Clin. Toxicol. 47 (2009) 89–100, http://dx.doi.org/10.1080/15563650802520675.

[34] H.X. Jiang, L.S. Chen, J.G. Zheng, S. Han, N. Tang, B.R. Smith, Aluminum-induced effects on Photosystem II photochemistry in citrus leaves assessed by the chlorophyll a fluorescence transient, Tree Physiol. 28 (2008) 1863–1871.

[35] J.M. Seitz, R. Eifler, F.W. Bach, H.J. Maier, Magnesium degradation products: effects on tissue and human metabolism, J. Biomed. Mater. Res. A 102 (2014) 3744–3753, http://dx.doi.org/10.1002/jbm.a.35023.

Isaiah Adekanmbi is an R&D Engineer at Depuy Synthes, working on orthopaedic medical devices for sensor enabled surgery. After receiving a First Class honours degree in Biomedical Materials Science and Engineering from Queen Mary University of London in 2006, he spent 3 years working at Nanoforce Technology Ltd. as an Engineer developing nanomaterials for medical, electronic and defence applications. He then completed his DPhil at the University of Oxford in Orthopaedic Engineering in 2013, before undertaking a Post-Doctoral Research Associate in Biomaterials for Paediatric Tracheal Stents at the University of Glasgow and subsequently became a visiting researcher at Columbia University.

Christopher Z. Mosher is a Ph.D. candidate in Dr. Helen H. Lu's Biomaterials and Interface Tissue Engineering Laboratory in the Biomedical Engineering department at Columbia University. His research focuses on integrative and functional cartilage repair in patients with osteochondral diseases, such as post-traumatic osteoarthritis. To achieve this, he is investigating polymer systems designed to integrate cartilage grafts currently used in the clinic with surrounding host tissues (cartilage and bone). Additionally, he is a recipient of the National Science Foundation Graduate Research Fellowship and has communicated his findings internationally through both publications and conference proceedings.

Helen H. Lu is currently a Professor of Biomedical Engineering and the Director of the Biomaterials and Interface Tissue Engineering Laboratory at Columbia University. Her research focuses on Orthopaedic Interface Tissue Engineering and the formation of composite tissue systems, with the goal of achieving integrative and functional repair of soft tissue injuries. Additionally, her research group is active in the design of novel biomaterials for orthopaedic and dental applications. Her group has published over eighty original research articles, invited reviews and book chapters in biomaterials and tissue engineering, and she is the inventor and co-inventor of more than a dozen patents and applications.

Mathis Riehle is a Reader and Director of the Centre for Cell Engineering at the University of Glasgow. After undergraduate and Doctorate training in cell biology at the Institute for Cinematic Cell Research (JW Goethe University Frankfurt) he moved to Scotland to join the interdisciplinary group of Prof Adam CG Curtis and Prof Chris DW Wilkinson in Glasgow. Now he works at the use of designed passive and active materials interfaces for nerve repair, acoustics to sort cells and structure constructs, and general studies into the cell/materials interface.

Haytham Kubba has been a Consultant in Children's ENT at Glasgow's Yorkhill Hospital since 2003, and is lead clinician for Scotland's National Service for Paediatric Airway Reconstruction Surgery. He graduated from the University of Newcastle upon Tyne in the North of England and trained in Glasgow with spells as a research registrar at the Medical Research Council's Institute for Hearing Research and clinical fellow at Great Ormond Street Hospital in London. His clinical interests are neurodisability, head and neck malformations and airway surgery.

K. Elizabeth Tanner is Professor of Biomedical Materials in the School of Engineering at University of Glasgow. She is also a visiting professor in the Department of Orthopaedics, Lund University Hospital, Sweden. She graduated in Engineering Science and then did her DPhil at the University of Oxford. She joined Queen Mary University of London progressing through to Professor in 1998. In 2007 she joined the University of Glasgow. In 2006 she was elected a Fellow of the Royal Academy of Engineering and in 2015 Fellow of the Royal Society of Edinburgh.